Duet model of predictive coding unifies diverse neuroscience experimental protocols

John H. Meng¹, Jordan M. Ross², Jordan P. Hamm^{2,3,4}, Xiao-Jing Wang^{1*}

*Corresponding author(s). E-mail(s): xjwang@nyu.edu

1 Summary

The brain continuously generates predictions about the external world, allowing us to rapidly detect and prioritize unexpected events, such as a mistuned piano note or an omitted one. Experimental studies have shown that neurons in sensory cortices respond to various types of contextual deviants across different protocols, and sensory response is not reduced to zero when a stimulus is fully expected. To account for diverse forms of observed deviations, here we introduce duet predictive coding, a minimal and biologically plausible framework in which functional subgroups of neurons encode positive and negative prediction errors separately. In contrast to classical predictive coding [34], which assumes top-down input is purely inhibitory, our theory posits that it is context-dependent rather than absolute. This model reproduces neural responses observed in diverse predictive coding paradigms across visual and auditory cortices. Critically, our framework predicts the existence of neurons tuned to negative prediction errors in the oddball paradigm, a prediction confirmed by our analyses, yet overlooked by classical predictive coding models. Our findings suggest that the brain's deviance detection relies on duet predictive error computation, offering a unifying explanation across seemingly disparate experimental protocols.

2 Introduction

In our daily lives, we consciously or unconsciously predict what will happen around us. We generate internal expectations and compare them with incoming stimuli, such as a sound or a visual pattern (Figure 1A). For example, when playing the piano, we can often predict the upcoming note and may disengage our attention from it. Consequently, an off-key note may catch us by surprise. Similarly, we can detect an out-of-tune sound during a live classical performance if we are familiar with the melody. In a simplified scenario, when our internal expectations and incoming stimuli align, we tend to ignore

¹Center for Neural Science, New York University, New York, 10003, NY, United States.

²Center for Behavioral Neuroscience, Georgia State University, Atlanta, 30303, GA, United States.

³Emotional Brain Institute, Nathan S. Kline Institute for Psychiatric Research, New York, 10962, NY, United States.

⁴Department of Psychiatry, New York University Grossman School of Medicine, New York, 10016, NY, United States.

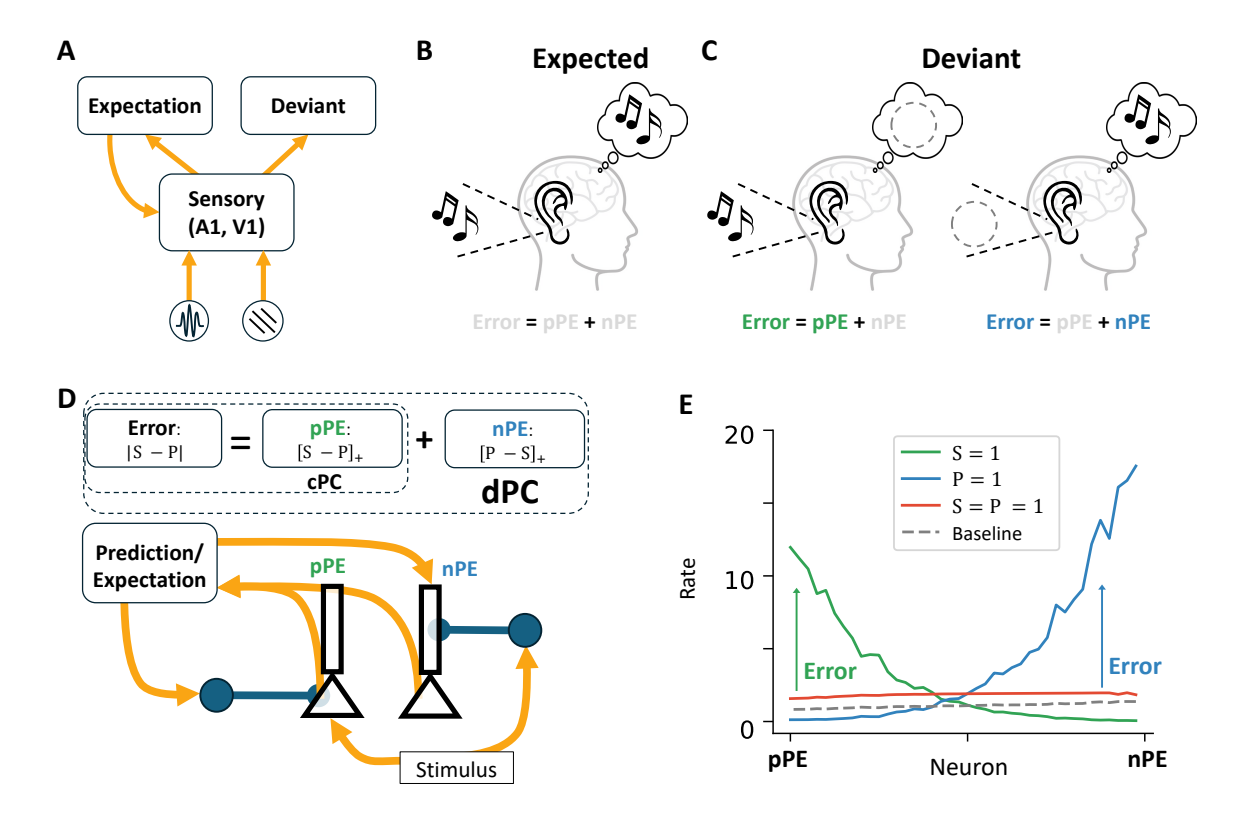


Fig. 1 Concepts of duet predictive coding (dPC). (A) Illustration of deviant computation by comparing the expectation with different types of incoming stimuli. (B) An expected case when the stimulus matches the internal expectation. (C) Deviant cases where (Left) stimulus is received without a corresponding expectation, or (Right) an expected stimulus is omitted. (D) Conceptual necessity in error calculation. Classic predictive coding (cPC) only considers positive prediction error (pPE), while dPC accounts for both pPE and negative prediction error (nPE). The pPE neurons are excited by the stimulus (S) and inhibited by the prediction (P) through local inhibitory neurons, encoding the positive error ($[S-P]_+$). Similarly, the nPE neurons are excited by the prediction and inhibited by the stimulus, thereby encoding the negative error ($[P-S]_+$). The required connectivity can be reached through local, biologically feasible learning rules [27, 18]. (E) Firing rates of neurons in different contexts after learning based on [27]. The overall firing rate is close to baseline when stimulus and prediction match. Importantly, in dPC, the prediction input is net excitatory when presented in isolation but becomes net inhibitory when paired with the stimulus.

the sensory input (Figure 1B). In contrast, when expectations and stimuli do not match, the brain may generate a deviance-related signal, enabling us to process the unexpected event with heightened vigilance or urgency (Figure 1C). This deviance signal may arise in two forms: when a stimulus occurs without a corresponding internal prediction, like an uninvited guest showing up, or when an expected stimulus fails to occur, as in the case of a speaker not showing up to a seminar. Both types of errors have been detected at the sensory areas [14, 15, 25, 24].

The mathematical formulation of deviance detection can be simplified as the computation of the absolute difference (error) between the incoming stimulus and the internal prediction signal. This error can be split into two components: the positive prediction error (pPE), representing the positive part of the absolute difference, and the negative prediction error (nPE), representing the remaining negative part (Figure 1D). Since neurons in sensory areas typically have low baseline firing rates [7, 30, 35], it is challenging for a single group to signal bidirectional changes, which are required for representing error. Historically, the classic predictive coding framework (cPC), developed by Rao and Ballard [34], included only pPE neurons to explain the reduced visual response to the same stimulus when it is expected, while allowing the units to have negative firing rates. The cPC model has also been used to

account for mismatch negativity (MMN) observed in fMRI and electroencephalography (EEG) [13, 48]. Over the years, several extensions and modifications of this framework have been proposed [29, 43, 28], yet most continue to focus solely on top-down inhibitory effects on pPE components. However, the notion that top-down input is purely inhibitory has been widely challenged [52, 9, 29, 10, 20]. This limitation constrains the cPC framework's ability to explain the neural response to omission [16, 25, 24].

To overcome the limitations of the cPC framework, one possibility is that two functionally distinct populations in the sensory area separately encode pPE and nPE, which we will refer to as the duet predictive coding (dPC) framework. Our previous work showed that pPE and nPE neurons can coemerge within a circuit via a local learning rule [27], explaining a broad range of motor-sensory phenomena under the dPC framework [1, 21, 3]. Similar connectivity patterns can be learned by enforcing excitation—inhibition balance at both the soma and dendrite of pyramidal cells [18]. The core idea of dPC is that neurons remain near baseline activity when stimulus and prediction co-occur, as in expected conditions (Figure 1E). When either input is presented alone, excitation in the driven population outweighs inhibition in the suppressed population, allowing the population to act as an effective error detector (Figure 1E). Unlike cPC, the overall effect of prediction input on the local sensory circuit is net-excitatory in isolation but becomes net-inhibitory when paired with a stimulus, making its inhibitory effect context-dependent rather than absolute.

Conceptually, including nPE neurons is counterintuitive because they encode the rectified difference between prediction and stimulus ($[P-S]_+$), which means some sensory-cortical neurons reduce their activity in response to the stimulus. Nevertheless, recent studies have observed nPE neurons in primary visual cortex (V1) during motion-visual mismatch [1, 21], audio-visual mismatch [11], and in auditory cortex during motor-auditory mismatch [42]. In these tasks, the self-generated motor signal acts as the prediction, compared against sensory input that either results from self-motion (closed-loop) or not (open-loop). Because sensory responses are reduced in closed-loop compared to open-loop conditions, these findings are taken as evidence supporting predictive coding theory [22]. Negative prediction errors arise when expected stimuli are interrupted during movement, such as when visual flow is paused while the animal runs on a treadmill in a virtual environment [1]. In such cases, population responses increase, and neurons that respond selectively to negative errors are identified as nPEs. Notably, these neurons also likely exhibit a shared transcriptomic profile that distinguishes them from pPE neurons [31].

However, the prediction signal is often considered an internally generated signal independent of motor output. In such cases, it arises from stimulus history rather than movement. For example, in classic MMN studies [44], EEG responses were stronger to rare tones than to frequent ones, when subjects remained still. Here, the prediction signal is thought to originate from prefrontal or other higher-order cortical areas [23, 13, 20]. If the transcriptomic subtype enriched for nPE neurons in motor-sensory tasks [31] is also present in these contexts, do they still function as nPE neurons when predictions are history-based? If so, how can they be identified and distinguished from pPE neurons?

In this work, we systematically investigate the role of nPE neurons under the dPC framework across diverse predictive coding paradigms using our model and analysis. We first show that the dPC framework explains omission responses via the nPE component [25, 24], and aligns with MMN literature [12]. We then demonstrate how the model captures single-neuron responses in oddball paradigms, predicting a joint contribution of pPE and nPE neurons during deviance detection. Importantly, the contribution from nPE is incompatible with the cPC framework [34]. Finally, our theory predicts distinct behavioral signatures that differentiate pPE and nPE neurons, which we validate through analyzing experimental data.

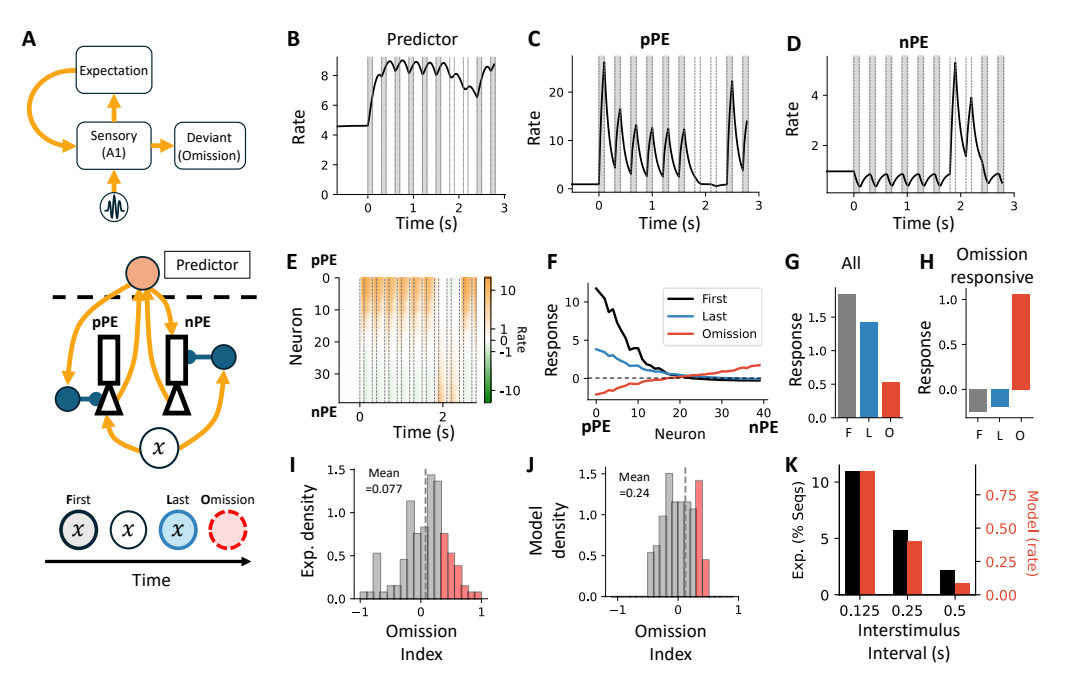


Fig. 2 dPC reproduces omission responses, since the predictor input is net excitatory if presented in isolation. (A) Top: A1 can generate omission responses by internal expectation. Bottom: We use a predictor to generate the prediction input. The model receives several repetitions of the same stimulus to build up the prediction before the omission. (B) Predictor activity over time. The grey shading indicates the stimulus periods. (C, D) Time courses of a pPE neuron and an nPE neuron. The omission response is contributed by nPE neurons. (E) Response of individual neurons compared to the baseline. The neurons are sorted based on the strength of stimulus input. (F) Neural responses at the first occurrence, last repetition, and during omission. (G) Average response over the population. (H) Average response restricted to omission-responsive neurons. (I, J) Distribution of omission of data (I) and the model (J). (I) is modified from [24]. The dashed line indicates the mean. The red shading highlights neurons with omission index > 1/3, indicating their response is at least twice the response during the last repetition. (K) Population-level omission response as a function of the interstimulus interval. See [24] for the definition of omission-responsive sequence. (J, K) are generated in the realistic model version. Here, $\tau_P = 0.1$ s.

3 Results

3.1 dPC reproduces omission response

Recently, studies by [25, 24] demonstrated that omission responses can be detected in single neurons in the primary auditory cortex (A1). In their experiment, a sound was presented repetitively at fixed time intervals, with occasional omissions—trials in which a sound was unexpectedly absent. Recordings from the mouse A1 revealed that some neurons consistently responded to these omissions. The authors hypothesized that mice formed an internal expectation of the upcoming sound with precise temporal resolution. When a predicted sound failed to occur, this internally generated prediction signal reached the auditory cortex and triggered the omission response. This suggests the top-down input excites the sensory area. This contradicts the cPC framework, which holds that top-down input is inhibitory.

We investigated this omission protocol within our dPC framework (Figure 2A). We used the learned local connectivity from our previous work [27] as the synaptic architecture. To simulate internal prediction originating from a high hierarchical area, we introduced a leaky integrator acting as a predictor, which generates the top-down prediction input (see Methods for details). This predictor receives bottom-up input uniformly from all neurons in the sensory area and operates on a slower timescale [5, 40] than individual sensory neurons. The top-down prediction signal is temporally aligned with the stimulus window, an essential feature for reproducing omission responses observed at precise expected time points in the experimental data. In our model, this temporal alignment is implemented

via a binary timing mechanism for simplicity. The precise timing can be achieved through spike-timing-dependent plasticity, as proposed in [48]. The stimulus is delivered at fixed intervals and adapted across repetitions. After a set number of repetitions ($N_{\text{rep}} = 6$ in this case), the stimulus is omitted, simulating an 'omission' trial.

In our model, the prediction input is net excitatory when presented in isolation, as in the omission case. This triggers the omission response naturally. In detail, the predictor starts with a high baseline firing rate of approximately 5 Hz [19] and saturates at 10 Hz. The predictor in simulation gradually builds up an internal expectation by integrating activity from the sensory area (Figure 2B), and generates corresponding top-down prediction input during stimulus periods. By our choice, a predictor with 10 Hz generates the maximum prediction input, as P=1 in Figure 1E. During omission trials, predictor activity decreases but remains above baseline, driving a prediction signal. Though the net effect is excitatory for the whole population, it has differential effects on pPE and nPE neurons. During stimulus repetitions, pPE neuron activity decreases due to both stimulus-driven adaptation and top-down inhibition from the predictor (Figure 2C). During the omission period, their activity remains close to zero. In contrast, nPE neurons, excited by the predictor and inhibited by the stimulus, respond differently. During the omission, prediction input persists while stimulus-driven inhibition disappears, resulting in a strong excitatory response in nPE neurons (Figure 2D). At the population level, nPE neurons exhibit strong excited activity, while the low baseline firing rate limits suppression in pPE neurons (Figure 2E, F). Thus, on average, the overall population response to omission remains positive (Figure 2G). Among omission-responsive neurons (Figure 2H; see Methods), the response is higher than the population average during omission, but suppressed below baseline during the first and last repetitions, reflecting that the nPE neurons are inhibited by the stimulus.

In the experiment by [24], the authors quantified omission responses using an omission index, defined as the firing rate difference between the omission and repeated stimulus conditions, normalized by their sum. An omission index of 1 indicates that a neuron responds exclusively to the omission, whereas an index of –1 indicates exclusive response to the repeated stimulus. They found that neurons exhibited a broad distribution of omission indices with a positive mean (Figure 2I), and a subset of neurons had indices greater than 1/3, suggesting that their omission response was at least twice as large as their response to the repeated stimulus. We successfully reproduced these signature properties in the realistic model (see Methods, Figure 2J). In this version, each cell receives a different total maximum input, making the model more biologically plausible but less straightforward to interpret. We use the realistic model for comparisons with experimental data and explicitly indicate whenever it is applied. Additionally, [24] reported that doubling the inter-stimulus interval halved the proportion of neurons with significant omission responses, suggesting that the internal predictor may function as a leaky integrator. This behavior is reproduced in our realistic model and supports our modeling choice for predictor dynamics (Figure 2K).

3.2 dPC reproduces key properties of mismatch negativity

Next, we study whether our dPC framework can explain the classic mismatch negativity (MMN) that is measured by the electroencephalogram (EEG) at the vertex of the scalp [44]. In a typical experiment, subjects are required to passively listen to a series of high-pitched tones and low-pitched tones and count the number of high-pitched tones in a block of 200 trials. The probability of high-pitch tones varied across blocks. When comparing the response to a high-pitched tone that follows a series of low-pitched tones to a control case in which the sequence contains only high-pitched tones, the EEG recordings show a larger response, reflected by the signature negative component peaking at 200 msec (N200), which is named as mismatch negativity (MMN). This signature is widely studied as a biomarker in diagnosing early psychosis [46]. Previous studies show that the MMN can be explained by a mass-type model [12, 13] that only describes the average population response and includes a top-down inhibitory effect through the pPE component. Does including the nPE component in dPC compromise the model's ability to explain MMN?

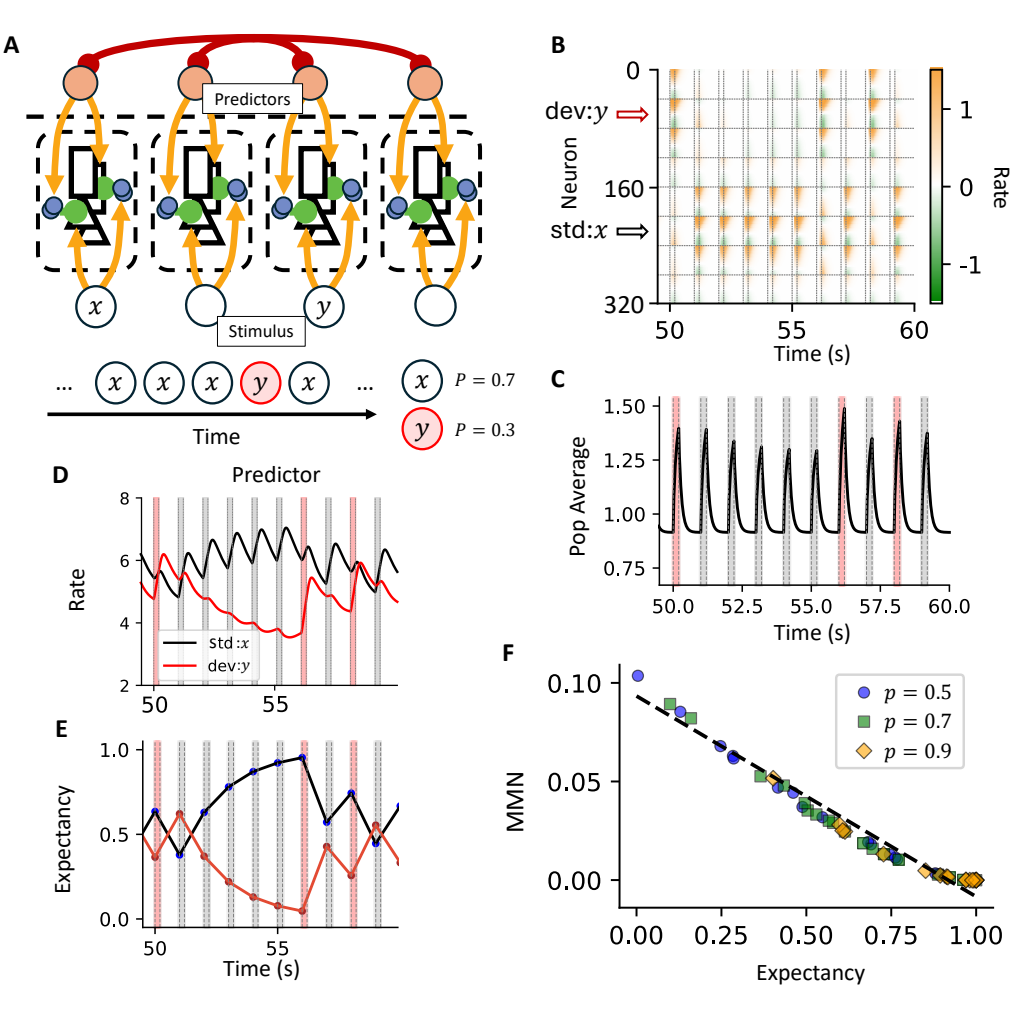


Fig. 3 dPC reproduces key properties of mismatch negativity, since predictor input is net inhibitory if it co-exists with the stimulus. (A) Model schematic. Multiple columns of pPE and nPE neurons are included, each selective to different stimuli. Standard and deviant stimuli are presented randomly according to specified probabilities. (B) Firing rates of individual neurons over time. Horizontal dashed lines separate neurons by stimulus selectivity. Vertical dashed lines mark stimulus onset and offset. (C) Average firing rate across the population. Red shading indicates deviant stimuli; gray shading indicates standard stimuli. (D) Predictor activity for both standard and deviant stimuli. (E) Expectancy of the standard and deviant stimuli over time. See Methods. (F) MMN is negatively correlated with expectancy. See the main texts for details. Different symbols represent data from different simulations. Symbols are downsampled for clarity, but fitting is performed on all data combined across runs. Here, $\tau_P = 1s$.

The dPC framework claims that prediction input is net inhibitory when paired with a stimulus, reproducing the signature behaviors in MMN. In our model, we include $N_{col} = 8$ columns, each tuned to a distinct stimulus frequency (Figure 3A), with a dedicated predictor. Each predictor receives excitatory input from $N_{pCol} = 40$ neurons in its column and sends the prediction signal back. Within each column, we include both pPE and nPE neurons, responding to the corresponding stimulus and predictor. We begin with a case where a standard stimulus x appears with p = 0.7, and a deviant stimulus with p = 0.3. The predictors operate with a longer time constant $\tau_p = 1$ s, compared to the omission case. These predictors further inhibit each other via bell-shaped lateral inhibition (see Methods).

In this model, individual neurons respond heterogeneously to the stimulus (Figure 3B). Neurons from different columns are stacked vertically, with each column separated by horizontal dashed lines.

Within each column, pPE neurons have smaller indices than nPE neurons. As expected, pPE neurons in the stimulus-matched column are strongly activated during the stimulus period, while nPE neurons within the same column are slightly suppressed. At the population level, the average activity in each column remains positive, as pPE excitation outweighs nPE suppression. In addition, the average population response varies with stimulus history (Figure 3C). Activity is highest for the deviant stimulus y, while responses to repeated presentations of the standard stimulus x gradually decline. This modulation reflects changes in predictor activity over time (Figure 3D): as x is repeatedly presented, predictor, activity builds up, leading to reduced activity in column x, since the prediction input is net inhibitory when paired with its corresponding stimulus. This pattern reverses when a deviant stimulus y is presented. Due to lateral inhibition, predictor, activity remains low while predictor, stays elevated. The resulting reduced inhibition from predictor, leads to a stronger response in column y. Notably, column x also shows a positive response when the deviant stimulus y is presented, as predictor, excites column x in the absence of stimulus x, mimicking an omission response. This will be discussed further in later sections.

A previous study [44] explained the MMN in a Bayesian framework by a latent "expectancy" variable, which estimates leaky stimulus history using a fitted memory decay rate α (Supplementary Figure 7A, see Methods). To test whether this expectancy also accounts for the activity changes in the model, we quantified MMN as the difference in population responses to a stimulus presented in a randomized sequence versus a fixed sequence containing only that stimulus (i.e., p=1). We found that MMN is linearly and negatively correlated with the latent expectancy (Figure 3E, F), agreeing with the experimental observation (Supplementary Figure 7A).

The degree of leakiness in calculating the expectancy is controlled by the decay rate α . To assess its robustness, we evaluated model fit using the explained variance R^2 (Supplementary Figure 7B). We found that $\alpha \in [0.5, 0.7]$ consistently produces a strong anti-correlation between expectancy and MMN. With our carefully chosen parameters, the optimal decay rate is $\alpha_{\text{leak}} = 0.6$, which matches the value reported in experimental data [44] (Supplementary Figure 7A).

To better illustrate how MMN increases with repetition, we tested our model using a fixed sequence of N_{rep} standard stimuli followed by a single deviant (Supplementary Figure 8). The longer the repetition sequence, the less expected the deviant stimulus. Here, stimulus presentation triggered heterogeneous responses across individual neurons (Supplementary Figure 8A, D), as seen previously. When comparing $N_{rep} = 6$ to $N_{rep} = 2$, the activity difference is larger across predictors dedicated to the standard and the deviant stimulus (Supplementary Figure 8B, E), resulting in a stronger MMN (Supplementary Figure 8C, F). MMN amplitude saturates around $N_{rep} = 5$ for predictor time constant $\tau_P = 1$ (Supplementary Figure 8G, as used in Figure 3). A smaller predictor time constant leads to faster MMN saturation with fewer repetitions (Supplementary Figure 8G), but the MMN saturates at a smaller amplitude (Supplementary Figure 8H).

3.3 dPC predicts nPE contributions in deviance detection tasks

Though MMN is often explained through predictive coding, an alternative account attributes it to fatigue-like mechanisms, such as stimulus-specific adaptation (SSA) [13]. To isolate top-down contributions, recent studies have focused on deviance detection (DD), which measures context modulation by comparing responses to the same stimulus presented either as a deviant or as a probability-matched control [14, 15, 4]. The control is typically the first occurrence of the stimulus (Figure 4A) or a version interleaved within a sequence of randomized stimuli, both minimizing adaptation effects. In this section, we focus on using the first occurrence as the control, and address the randomized control in the next section. In addition to the population activity, advances in techniques like calcium imaging now enable measurement of individual neuron activity. While deviance detection at the single-neuron level is variable and heterogeneous [14, 15], can this heterogeneity be dismissed as random noise, as in mass models [12] that describe only population-averaged responses? Or is it functionally meaningful for computing predictive error?

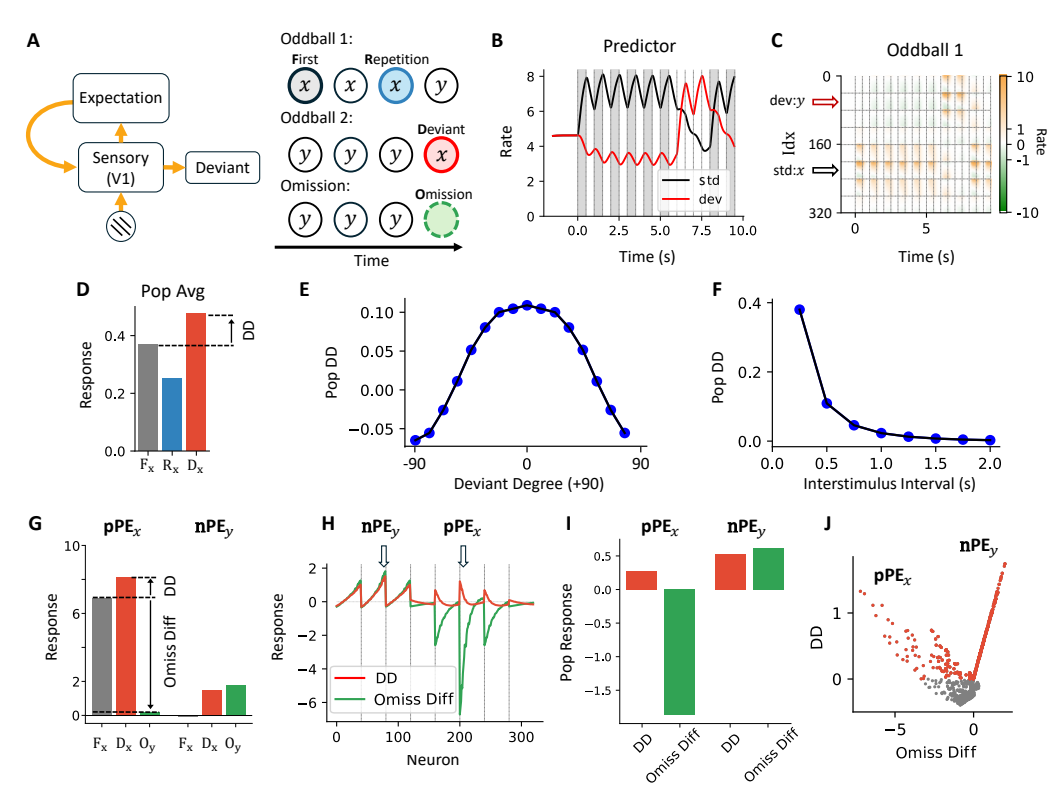


Fig. 4 dPC predicts functional role of nPE neurons in deviant detection. (A) Left: V1 can generate deviance detection signals in an oddball protocol. Right: simulation schematic. Responses to the same stimulus presented in different contexts (first, repetition, deviant, or omission) are compared. (B) Predictor activity in the corresponding standard (black) and deviant sequences (red). (C) Firing rates of individual neurons in oddball sequence 1. (D) Average population activity across different contexts within the oddball sequences. (E) Population DD response decreases as the orientation of the deviant stimulus diverges from the perpendicular phase. (F) The population DD response decreases with increasing stimulus interval. (G) Firing rates of an example pPE $_x$ neuron and an example nPE $_y$ neuron when stimulus x is presented as the first occurrence, as a deviant, or is omitted. (H) Single neuron responses. The red line indicates the deviance detection, and the green line indicates the omission difference, calculated as the difference between the omission response and the response at the first occurrence. (I) DD and omission differences of pPE $_x$ and nPE $_y$ population. While both show positive DD responses, only the nPE $_y$ population exhibits an omission response greater than the first occurrence. (J) Scatter plot of DD versus omission difference. (I, J) are generated from the realistic model version. See Methods. Here, $\tau_P = 0.4s$.

Our dPC framework reproduces DD responses at both the population and single-neuron levels in sensory areas such as V1. The network structure remains the same as in Figure 3A, but we use a shorter predictor timescale ($\tau_P = 0.4$ s) and include stimulus adaptation across repetitions (see Methods). To test whether neural responses reflect contextual change, we simulate two oddball sequences: sequence no. 1 (xxxy) where stimulus x appears repeatedly until the deviant y, and sequence no. 2 (yyyx) where x is the deviant (Figure 4A). Stimuli x and y represent orthogonal grating orientations. We also test omission responses using the sequence yyyo with the same number of repetitions in oddball sequence no.1 and no.2.

In later sections, we label stimulus presentations in different contexts as follows: F_x denotes the first occurrence of stimulus x, R_x denotes the fourth or later repetitions, and D_x indicates that stimulus x is presented as a deviant. Analogous notations F_y , R_y , and D_y apply to stimulus y. Omissions in sequences xxxo and yyyo are labeled O_x and O_y , respectively. We refer to oddball sequence no. 1 as the standard sequence for x and oddball sequence no. 2 as the deviant sequence, with terminology applied symmetrically for y.

As shown earlier in the MMN case, predictor activity increases across repetitions when the corresponding stimulus is presented in the standard sequence, but decreases when the corresponding stimulus is presented in the deviant sequence due to lateral inhibition (Figure 4B). Their activities, which are different across contexts, modulated the neuron response to the same stimulus (Figure 4C). As a whole population, the sensory response to R_x is below that to F_x , and it is larger to D_x than to F_x (Figure 4D). Population-level deviance detection to stimulus x (DD), quantified as the response difference to D_x and F_x , varies with the angular difference between stimuli x and y (Figure 4E). Maximum deviance detection occurs when x and y are orthogonal. As the angular difference decreases, DD diminishes. When the angular difference reaches zero, the DD flips sign, reflecting that D_x and R_x become the same. Similar to the trend observed in the omission protocol, DD decreases exponentially with increasing inter-stimulus interval, reflecting the decaying memory of the predictor (Figure 4F). The prediction on how DD changes over the angular difference and interstimulus interval can be tested in future experiments.

At the single-cell level, unlike the context-dependent modulation seen at the population level, the predictor consistently inhibits pPE neurons and excites nPE neurons within the same column (Supp. Figure 9A, B). Since predictor activity is higher during R_x than F_x , and lower during D_x than F_x , the pPE_x neuron is more inhibited in the repeated condition and less inhibited in the deviant condition. In contrast, the nPE_x neuron is more excited during R_x and less excited during D_x , though its overall response is smaller than that of pPE_x. The activity of all neurons in the x-selective column is shown in Supp. Figure 9C, D. Since the reduced response to R_x could arise from both stimulus-specific adaptation and top-down modulation, we tested a condition without adaptation (Supp. Figure 9E). In this case, the reduction in response to R_x is attenuated, while the increase in response to D_x remains unchanged, suggesting that DD may be a more reliable readout of top-down prediction than MMN.

As suggested in the previous section, the population-level DD response during D_x arises from two distinct sources in the model. The first is reduced inhibition from the predictor in the x-selective column, as previously discussed. The second originates from the omission-like response in the y-selective column, where predictor y exerts a net excitatory effect, particularly on nPE_y . Notably, nPE_y shows a DD response comparable to pPE_x , but its response to F_x is much weaker (Figure 4G). This highlights a potential confound: if we define DD solely by comparing D_x and F_x , we might mistakenly classify nPE_y as a pPE_x neuron, even though nPE_y does not respond to stimulus x.

Next, we find that a commonly utilized omission protocol can evoke responses that clearly differentiate pPE_x and nPE_y neurons (Figure 4A, G), as only nPE_y neurons respond to omission O_y , whereas pPE_x neurons do not (Figure 4H). In simulations using the realistic model, both populations exhibit DD responses, but only nPE_y neurons respond more strongly to O_y than to F_x . When plotting individual neuron activity along DD magnitude and response to O_y , the two populations form distinct branches (Figure 4J). This separation between pPE_x and nPE_y provides an experimental prediction that should be tested in future studies.

Lastly, a detailed decomposition of input contributions to both pPE_x and nPE_y across different protocols is shown in Supplementary Figure 10.

3.4 dPC predicts distinct pPE and nPE responses in a randomized oddball protocol

The difference between pPE_x and nPE_y neurons can be further tested in a randomized oddball protocol by comparing responses to the first occurrence (F_x) and to a control condition (C_x) in addition to using the omission protocol (Figure 5A). Here, the first occurrence F_x refers to the presentation of standard stimulus x immediately following the deviant stimulus y within a long sequence, not the first appearance of x in the entire run (Figure 5A). In [14, 15, 4], a many-standard sequence was used as the control instead of the first occurrence to avoid potential novelty effects. In the many-standard control, eight differently oriented gratings, including those used in the oddball sequences, are presented with equal probability. This design helps eliminate the influence of adaptation and expectation signals on

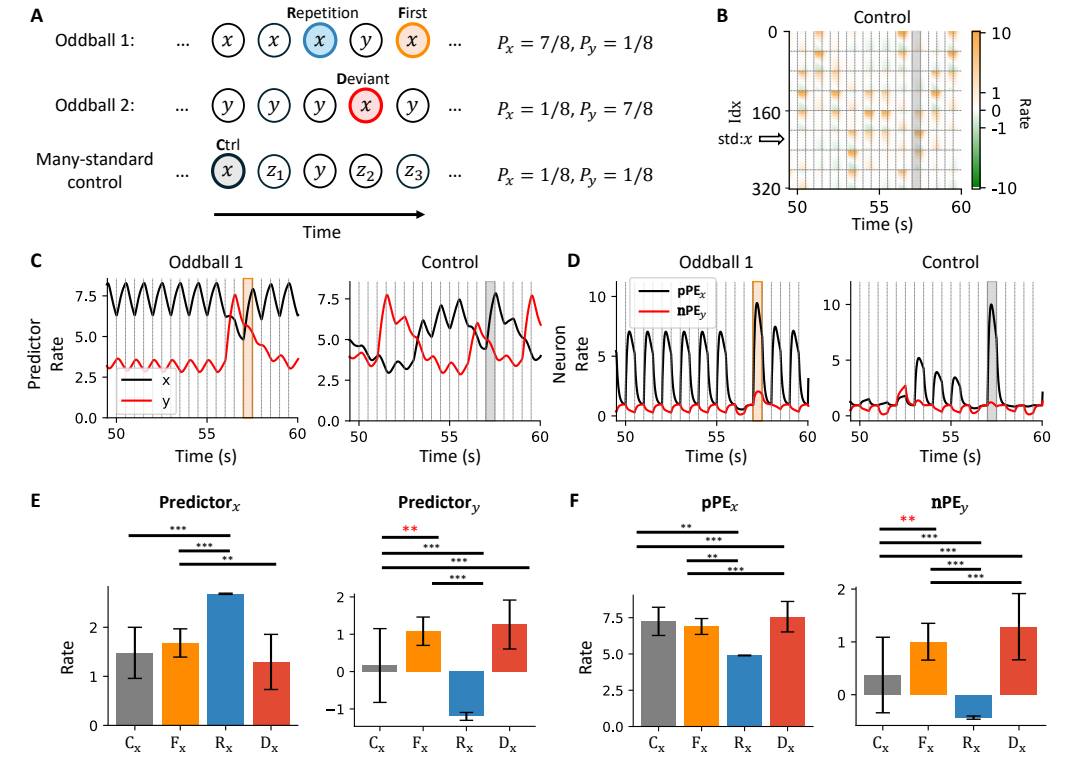


Fig. 5 nPE $_y$ neurons show stronger responses to F $_x$ than it to C $_x$. (A) Simulation schematic. The comparison focuses on the first stimulus presentation versus the stimulus in the many-standard control condition. (B) Activity of individual neurons in the many-standard control condition. The gray shading indicates when stimulus x is presented. (C) Predictor activity during oddball sequence one (left) and the many-standard control (right). Orange shading indicates the F $_x$, and gray shading indicates the C $_x$. Activity for predictor $_x$ and predictor $_y$ is shown. (D) One pPE $_x$ and one nPE $_y$ activity during the oddball sequence 1 (left) and many standard controls (right). (E) predictor $_x$ and predictor $_y$ responses compared to the baseline across the C $_x$, F $_x$, R $_x$ and D $_x$ contexts. Activity of predictor $_y$ is significantly more larger during F $_x$ than during C $_x$. The error bar indicates the standard deviation. **: p < 0.01; ***: p < 0.001. (F) Activity of a pPE $_x$ and nPE $_y$ neuron across conditions. The activity of nPE $_y$ neuron is significantly larger during F $_x$ than during C $_x$. Detailed p-values are provided in the Supplementary Materials.

neural responses. The oddball sequences are randomized such that the number of repetitions between two deviants varies, rather than being fixed, to further minimize expectation-related effects. Here, we apply the same protocol to test our model. Individual neuron responses in the many-standard control sequence are shown in Figure 5B.

As before, predictor activity reflects a leaky integration of stimulus history (Figure 5C). In odd-ball sequence no. 1, since stimulus x occurs more frequently, predictor_x maintains elevated activity throughout most of the sequence, while predictor_y becomes active only when stimulus y appears. By definition, F_x follows D_y . During F_x , predictor_x begins to ramp up, and predictor_y starts to decline. However, due to the predictors' long timescale, predictor_y remains elevated during F_x compared to R_x . In contrast, under the many-standard control protocol, predictor activity stays near baseline unless the corresponding stimulus is presented, reflecting the randomized nature of the sequence.

When comparing predictor activity across all trials and contexts, the predictor_x does not differ significantly between C_x and F_x , whereas predictor_x shows a significant increase during F_x (p < 0.01, Welch's t-test; Figure 5E). This pattern is mirrored in the responses of pPE_x and nPE_y neurons: only the nPE_y neuron shows a significantly higher response (p < 0.01) during F_x than C_x , but not the pPE_x neuron (Figure 5D, F).

All pairwise p-values are reported in the Supplementary Materials.

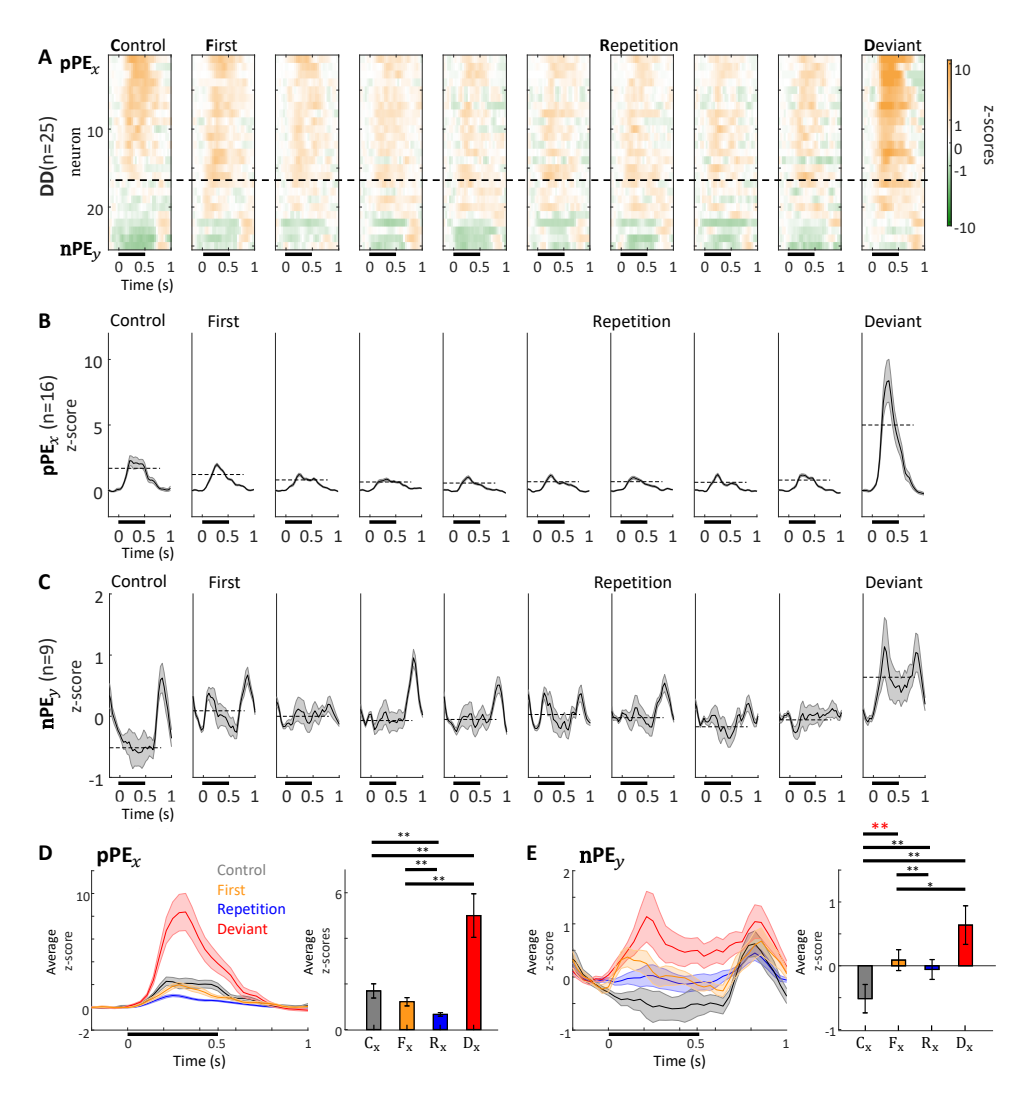


Fig. 6 Putative pPE_x and nPE_y neurons are both observed in an oddball paradigm experiment. (A) Activity of all identified deviant detector (DD) neurons (n=25) in the recorded population. DD neurons are defined as those that respond significantly more strongly to the deviant than to the control stimulus (p<0.05). Neurons above the dashed line also show a significant response in the many-standard control condition (p<0.05) and are considered as pPE_x neurons. The remaining neurons, which do not respond significantly in the control, are classified as nPE_y neurons. Neurons are sorted based on average activity during the control period. The black bar below the x-axis indicates the stimulation period. (B) Average z-scored activity of pPE_x neurons (n=15) across different contexts. (C) Average z-scored activity of nPE_y neurons (n=9) across different contexts. (D) Left: Overlay of z-scored pPE_x neuron responses across contexts. Right: Mean z-score during the stimulus period. The error bar indicates the standard error. No significant difference is observed between C_x and F_x (p>0.05). (E) Same as (D), but for nPE neurons. The activity during F_x is significantly larger than during C_x . *: p<0.05; **: p<0.01; ***: p<0.01; ***: p<0.001.

3.5 dPC predictions are confirmed in the experiment

Our model pinpoints predictions that can be experimentally tested. We have argued that both pPE_x and nPE_y neurons contribute to deviance detection and, therefore, should both exhibit stronger responses to deviant stimuli than to the many-standard control. Additionally, in contrast to pPE_x neurons, nPE_y , responding to $[P_y - S_y]_+$, should not respond to the tested stimulus in the control condition C_x . Furthermore, nPE_y neurons should respond more strongly during F_x than during C_x . We tested these predictions using both previously published data [4] and newly collected recordings,

comprising a total of N=326 stimulus–neuron pairs from three mice of either sex. The average responses of these neurons are shown in Supplementary Figure 11A–C. In these experiments, a 0.5s stimulus was presented to the animals with jittered inter-stimulus intervals ranging from 0.4 to 0.6s. The detailed experimental procedure is described in [4].

Among these neurons, 25 out of a total N=326 showed significantly stronger responses in the deviant context compared to the control (p<0.05, Welch's t-test; Figure 6A, Supp. Figure 11D-F). We refer to these as deviant detectors (DDs). This proportion is consistent with other reports during basic oddball paradigms [15, 4]. Within the DD population, 16 neurons also showed significant responses to the control condition (p<0.05, paired t-test), while the remaining 9 did not (p>0.05). We classify the former as pPE_x neurons and the latter as nPE_y neurons, since only pPE_x neurons are expected to respond in the control condition.

On average, the pPE_x neurons reproduce the response pattern previously reported [14, 15, 4] (Figure 6B), showing similar responses during C_x and F_x . Their activity decreases with repeated presentations but increases in D_x . In contrast, the nPE_y neurons (Figure 6C) exhibit a slightly suppressed response in the control condition. Their responses are larger during F_x and even more elevated during D_x .

When examining average responses across the stimulus period (Figure 6D), pPE_x neurons do not show a significant difference between C_x and F_x . In contrast, nPE neurons have significantly higher activity during F_x than C_x (p < 0.05, paired t-test; Figure 6E). This pattern can only be explained by top-down excitatory prediction input, which is incompatible with the cPC framework that considers top-down effects to be purely inhibitory. Importantly, our nPE neurons also cannot be interpreted as predictor neurons under cPC. In the cPC framework, predictor neurons reflect internal expectations and should respond strongly to the repeated stimulus, which is not observed in our data (Supp. Figure 11J–L).

In addition, we observed several differences in the average response time course. For nPE_y neurons, response onsets in the deviant context often occur slightly (about 100ms, or 3 frames in the recordings) before stimulus onset (Figure 6E), which is consistent with the idea that prediction signals arrive in advance of sensory input, reflecting internal expectation. These neurons also exhibit a rebound in activity following the stimulus period. One possible explanation is that the nPE_y population is nonspecifically inhibited by the stimulus (i.e., a nPE_y neuron can be inhibited by both stimulus x and y), and that removal of the stimulus disinhibits the neurons, leading to rebound activity.

In our model, orientation selectivity is explicitly imposed, and this is supported in the motion-visual mismatch experiment [53]. However, this constraint may not hold universally. To investigate this, we measured the tuning curves of pPE and nPE neurons based on their responses in the many-standard control condition (Supp. Figure 12A, B). We found that pPE neurons are more selective for orientation, exhibit greater response variability across orientations, and display higher average response power (Supp. Figure 12C). These results suggest that pPE neurons are more stimulus-selective, while nPE neurons are more indifferent to the content of the sensory input.

4 Discussion

Here, we propose a duet predictive coding (dPC) framework that unifies diverse neuroscience protocols across timescales and brain regions. This framework emphasizes that both positive prediction error (pPE) and negative prediction error (nPE) are theoretically essential to predictive coding and are supported by experimental evidence. Our model explains a wide range of phenomena, including motion-selective modulation of auditory responses [27], motor-visual mismatch [27], omission responses (Figure 2), mismatch negativity (Figure 3), and deviance detection in the oddball paradigm (Figure 5). Motivated by our theory and past work in motor-sensory predictive paradigms, we examined and confirmed putative nPE neurons, which were not previously acknowledged in the oddball context (Figure 6). Furthermore, we predict that the activity of pPE and nPE populations should

diverge more clearly in an omission protocol (Figure 4), a hypothesis that can be tested in future experiments.

The pioneering work of Rao and Ballard [34] shifted the prevailing view of the sensory cortices from a passive information-processing machine to an active organ of inference [9, 20]. In their formulation, top-down input represents predictions about the external world. Incoming sensory signals are compared against these internal predictions, and only the residual difference—i.e., the prediction error—is propagated to higher levels of the cortical hierarchy. However, this classic predictive coding (cPC) framework, along with its subsequent extensions, has been challenged on several fronts [9, 17, 10, 29]. First, cPC assumes that top-down predictions inhibit bottom-up sensory input, whereas corticocortical feedback and intralaminar interactions are predominantly excitatory. Although disynaptic inhibition, via excitatory drive of local GABAergic interneurons, can account for this discrepancy, cortico-cortical feedback also synapses on excitatory neurons [52], and activates both inhibitory and excitatory neurons [4]. Second, the original model allows negative firing rates, enabling excitatory neurons with low baseline activity to signal bidirectional changes, but at the cost of biological plausibility. Finally, the framework has been criticized for its limited ability to generate testable predictions, reducing its utility in guiding experimental research.

Our work suggests that duet predictive coding (dPC) can address limitations of previous models by incorporating negative prediction error (nPE) neurons into the circuit. Inspired by recent experimental findings [1, 22] and computational models [18], we previously argued that a biologically plausible local learning rule can give rise to optimal connectivity for computing prediction errors. This learned connectivity can further explain experimental observations such as motion-modulated suppression and motor-visual mismatch in the context of corollary discharge [27]. In our model, neurons exhibit low baseline firing rates, from which they can be robustly excited but only weakly inhibited. Consequently, top-down input is inhibitory only when paired with an expected stimulus but becomes excitatory in other contexts (Figure 1E). In other words, top-down inhibition is context-dependent rather than absolute.

Under this dPC framework, the deviant response in oddball protocols can be conceptually divided into two components: reduced top-down inhibition to the unexpected stimulus (stimulus x in the sequence yyyx) and top-down excitation to the omitted stimulus (no stimulus y during deviant in the sequence yyyx). These effects are mediated respectively by pPE neurons tuned to the unexpected stimulus and nPE neurons selective to the predictor associated with the omitted stimulus. Based on this theory, we identified putative nPE neurons that contribute to deviance detection in the oddball paradigm (Figure 6) and further predict that these nPE neurons will become more clearly distinguishable when combined with an omission protocol (Figure 4).

In our model, the predictors are modeled as mutually inhibited leaky integrators with a long time constant and baseline firing rates around 5Hz. This choice is mainly for simplicity, but requires further evidence from experiments to elucidate. Supporting that, the prefrontal cortex is observed to have a higher baseline firing rate [41, 19] than sensory areas, especially in the superficial layer 2/3 [7, 30, 35]. This suggests that a single predictor neuron at a higher hierarchical region can signal the expectancy change by increasing or decreasing its firing rate. However, this is not the only possibility. Theoretically, different pools of neurons can indicate the increasing or decreasing of internal expectancy as we split the prediction error neurons into pPE and nPE. Furthermore, the predictors may have attractor dynamics instead of leaky integrators. Currently, we choose the leaky integrator because the error signal decays away with longer interstimulus intervals in a passive task [24]. However, the predictions may be generated from attractor dynamics, especially when the internal prediction must be held to perform an active task, like delayed-match-to-sample tasks [38, 51]. In addition, the internal prediction may be coded through synaptic mechanisms [45, 32]. Finally, as we argued in our previous work [27], internal predictions may be generated ad hoc, as in the cases of corollary discharge. For example, when riding a bicycle on a rocky mountain trail, internal predictions of the visual field are continuously updated to account for self-motion and environmental changes. In such situations, precise predictive representations may be transient and do not require maintenance over seconds. In

summary, the detailed mechanisms of prediction generation require further study, and they are likely to differ across contexts.

If predictions are generated through different mechanisms in distinct brain regions, are pPE and nPE neurons drawn from the same neuronal pool across experiments? Our previous work [27] argued that the learned pPE or nPE identity of each neuron is determined by the initial ratio of excitatory input from stimulus versus prediction. If the prediction input arises solely from a corollary discharge signal, then pPE and nPE identities should remain stable as long as predictions map consistently onto the same motion signal. In the current study, the stimulus source remains constant, but the prediction source may vary. Since pPE neurons require strong stimulus input, we argue that the pPE population should be conserved across protocols. This is also consistent with the fact that the pPE neurons were strongly orientation selective (Supplementary Figure 12). However, if the prediction source differs, the corresponding nPE population may shift. In our model, we treat variability in input strength as heterogeneity, but recent work suggests that transcriptomic identity may also shape error signaling: specifically, L2/3 Rrad or Baz1a pyramidal neurons are enriched for pPE responses, while Adamts2 neurons preferentially exhibit nPE responses [31, 6]. These findings raise the possibility that pPE and nPE neurons may be further distinguished by their molecular and transcriptomic profiles.

Similarly, what are the identities of the two interneuron populations in our model? From a modeling perspective, the simplest approach is to assume an excitation-inhibition balance at both the soma and dendrites [18] or to posit a division of labor across interneuron subtypes [49]. Based on these assumptions, dendrite-targeting somatostatin-positive (SST) interneurons (INs) are likely to mediate stimulus-driven inhibition, while soma-targeting parvalbumin-positive (PV) interneurons are wellpositioned to relay prediction-related inhibition [47]. The role of SST cells in delivering stimulus-related inhibition to nPE neurons is supported by studies on motion-visual mismatch [1, 50, 22]. However, the identity of IN subtypes responsible for relaying top-down prediction remains less clear. In the auditory cortex, motion-related inhibition has been attributed to PV interneurons [36, 37]. Yet, recent findings suggest that this pathway may reflect a homogeneous gain control mechanism rather than balancing excitation from a specific predicted stimulus [3]. Although SST cells are generally less directly activated by long-range cortical inputs [26], emerging evidence indicates that they may, in some cases, be more responsive than PV cells in certain top-down signaling pathways [39]. Their involvement in pPE calculation is also supported in both auditory [37, 3] and visual studies [14]. Another major interneuron subtype, vasoactive intestinal peptide-positive (VIP) cells, typically inhibit SST cells and disinhibit pyramidal neurons [33, 52], making them less likely to mediate top-down inhibition directly. However, our recent findings suggest that a subpopulation of VIP interneurons co-expressing the neuropeptide cholecystokinin (CCK) can directly inhibit pyramidal cells with synaptic strength comparable to that onto SST cells, implying a potential role in mediating top-down inhibition [8]. In summary, the identity of interneurons responsible for relaying top-down inhibition remains unresolved. Given that internal predictions can arise via diverse mechanisms and pathways, it is plausible that top-down inhibition is mediated by a combination of IN subtypes rather than a single, dedicated class.

Classic predictive coding (cPC), developed from a normative framework, falls short in accounting for a range of experimental observations. In this work, we proposed duet predictive coding (dPC) with both positive prediction error (pPE) and negative prediction error (nPE) neurons as an extension of cPC to bridge the gap between theory and diverse experimental protocols. Our framework provides new insights into the generality of predictive coding across brain systems, elucidating how internal prediction signals guide the processing of incoming stimuli.

Methods

4.1 Sensory area

In this work, the single-neuron and synapse models within the sensory area are the same as in our previous study [27]. The connectivity within each column also follows the learned connectivity from

[27]. The neuron index within each column is sorted based on the input strength of the preferred stimulus. When showing the example traces, the pPE example neuron is always the neuron with the smallest index (maximum stimulus input strength), and the nPE example neuron is the one with the largest index (minimum stimulus input strength).

We employ two versions of the model in this study. The simplified version assumes homeostasis, meaning that the total maximum input from stimulus and prediction is equal across neurons. This version includes a small number of neurons per column $(N_{pCol}=40)$ and is used throughout most of the paper. It offers a more interpretable framework for illustrating the core mechanisms of dPC. The realistic version, in contrast, is designed to match experimental statistics and render testable predictions from theory. This version includes more neurons per column $(N_{pCol}=200)$, and it does not assume homeostasis. While it is less intuitive for illustrating mechanisms, it is essential for capturing biological variability, especially since homeostasis is not guaranteed in vivo, as seen in studies of selective modulation of auditory responses [3, 2]. Throughout the paper, we use the simplified version by default, and results from the realistic version are always explicitly stated.

In the following sections, we adopt the same notations as in [27]. In addition, we introduce predictors that generate top-down prediction inputs, and we extend the model to include multiple columns with different orientation selectivity. The specific modifications are described below:

4.2 Predictor

The pyramidal cells within a column are connected to an integrator with the same preferred orientation and homogeneous connectivity strength $g_{Int,E}$. These integrators are modeled as

$$\tau^{Int} \frac{dR}{dt} = -R + f^{Int}(I) \tag{1}$$

where τ^{Int} has a much longer time constant. The activation function here is a saturated version of the previous activation function f:

$$f(I) = \frac{\Delta V}{\tau(V_{th} - V_{reset})(1 - exp(-a\Delta V/\sigma_V)}$$
 (2)

with $\Delta V = I/g_L + V_l - V_{th}$ and the saturation as follows:

$$f^{Int}(I) = 10(1 - exp(-f(I)/10)) \tag{3}$$

With this choice, the activity of the integrator is capped at 10Hz, which is the maximum firing rate for the predictor in the previous model [27].

The integrators mutually inhibit each other through a bell-shaped connectivity.

$$W_{ij}^{IntInt} = J_{max} exp\left(-\frac{(\phi_i - \phi_j)^2}{\sigma_{Int}^2}\right) + J_{min}$$
(4)

Here, J_{min} is negative to represent lateral inhibition. For simplicity, we don't split recurrent excitation and inhibition in different connectivity matrices.

4.3 Simulated stimulus input

The stimulus input to individual neurons within the same column is drawn from a linearly uniform random distribution ranging from zero to a maximum value g_{max}^S , as in our previous work [27]. In simulations involving multiple columns, the maximum input is scaled based on the angular difference

between a neuron's preferred orientation (frequency) $\phi^{i_{col}}$ and the stimulus orientation (frequency) ϕ^{0} , using a Gaussian kernel:

$$g_{max}^{S,i_{col}} = g_{max}^{S} exp(-(\phi^0 - \phi^{i_{col}})^2 / \sigma_S^2)$$
 (5)

With σ_s is the width of the Gaussian kernel.

In the fixed oddball protocol, we simulate the model with stimulus S_x (standard stimulus), presented at a fixed orientation for eight repetitions. Each stimulus is shown for a duration t_S , with an inter-stimulus interval of t_{Int} . Following the eighth repetition, we present an orthogonal stimulus S_y as the deviant. This sequence is repeated twice and then followed by two additional standard trials with S_x . In the omission protocol, the deviant stimulus is replaced with an omission (i.e., $S_y = 0$). In the randomized oddball protocol, the stimulus on each trial is determined probabilistically based on the assigned probabilities P_x and P_y .

In the fixed oddball and omission protocols, adaptation is modeled by directly reducing the maximum stimulus conductance (g_{max}^S) for repeated stimuli.

$$g_{max}^{S,i_{rep}} = g_{max}^{S}(1 - d_{adap}(1 - r_{adap}^{i_{rep}-1}))$$
(6)

In the simulation matching MMN (Figure 3), adaptation is set to zero ($d_{\text{adap}} = 0$), based on lesion study findings [23], and is also omitted in the randomized oddball sequences.

4.4 Top-down prediction input

In our model, we include a prefrontal cortex (PFC)-like circuit composed of leaky integrators that accumulate temporal information. We assume that each predictor j projects only to its corresponding sensory column, generating mismatch receptive fields that match that of the sensory receptive field [53]. The top-down connectivity is the same as the learned connectivity matrix W_{ij} in our previous work [27], where j indexes the j-th predictor and i belongs to the j-th column.

These predictors excite the dendrites of pyramidal cells as well as the interneuron population I_2 . Experimental evidence suggests that top-down predictions may exert their influence with temporal precision, such that the sensory area receives prediction input only when it is computationally relevant for local processing. This timed prediction input could be implemented biologically via spike-timing-dependent plasticity (STDP), as proposed in [48]. For simplicity, we implement it as a binary timing in our model: the top-down excitation deviating from baseline is only applied when a stimulus is either presented or expected.

$$g_j = W_{ij} R_0^{int} + W_{ij} (R_j^{int} - s_0) \mathbb{I}_S, \tag{7}$$

 $\mathbb{I}_S = 1$ when any stimulus is presented. In the omission protocol, we also set $\mathbb{I}_S = 1$ when the model is "expecting" a stimulus.

4.5 Data analysis

In the auditory omission response analysis (Figure 2), we use the same omission index to quantify the distribution of population responses as in [24]. Specifically, for each cell, let r_s denote the response to the last stimulus presentation, and r_o the response to the omission. The omission index is defined as: iOMI = $(r_o - r_s)/(r_o + r_s)$. In our model, omission-responsive neurons are defined as those whose response during the omission period is at least twice as large as during the pre-omission period.

In reproducing MMN (Figure 3), we used a similar method to calculate "memory-based expectancy" M_s as in [44]: $M_{S=x}^{(t)} = \lambda \sum_{i=1}^{10} \alpha^i \mathbf{I}_{S=x}(S(t-i))$, with \mathbf{I}_s is an identity function where $\mathbf{I}_{S=x}(x) = 1$ and $\mathbf{I}_{S=x}(y) = 0$, and the normalization factor $\lambda = 1/\sum_{i=1}^{10} \alpha^i$.

In analyzing pPE and nPE population responses in the model, a neuron is labeled as a pPE neuron if it shows a positive deviance detection and a negative omission difference. Conversely, it is labeled as

an nPE neuron if both the deviance detection and omission difference are positive. After classification, activity is averaged separately across the pPE and nPE populations.

To test whether nPE neurons play a functional role in the oddball paradigm, we analyzed experimental data from mice of either sex (n=3), including previously published recordings from [4]. Detailed procedures for data collection and z-score normalization are described in [4]. The total number of cell–stimulus pairs examined was 326. A cell was classified as responsive only if its response to a stimulus in the many-standard control condition was significantly greater than its pre-stimulus baseline (p < 0.05). We then focused on the subset of responsive cells that showed significantly higher activity in response to the same stimulus in the deviant context compared to the many-standard control (p < 0.05). All p-values for single-cell comparisons were corrected using the Benjamini–Hochberg (BH) procedure.

Code Availability

We analyze the model-generated data using Python 3.9 and the experimental data using MATLAB R2024b. All analysis code will be made available on GitHub upon acceptance.

Declaration of generative AI and AI-assisted technologies in the writing process

During the preparation of this work, the authors used ChatGPT-40 in order to assist with proofreading and improving the clarity of the manuscript. After using this tool, the authors reviewed and edited the content as needed and take full responsibility for the content of the publication.

Author contributions

J.H.M. and X.J.W. conceptualized the project. J.H.M. performed simulations, data analyses, and wrote the manuscript. J.M.R. and J.P.H. collect the sample. J.P.H. and X.J.W. supervised the study. All authors contributed to editing and finalizing the manuscript.

Acknowledgement

We thank Aldo Battista, Yue Liu, Tianshu Li, and other members of Xiao-Jing Wang lab for the discussion. We thank Cristina Savin and David Schneider for their suggestions and feedback on an early version of the manuscript. We thank Kevin Berlemont for an early exploration of this project. This work is supported by ONR grant N00014-23-1-2040 and NIH grant R01MH062349 (to XJW), and NIH grant R01EY033950 from the National Eye Institute (to JPH)

References

- [1] Alexander Attinger, Bo Wang, and Georg B Keller. "Visuomotor coupling shapes the functional development of mouse visual cortex". In: Cell 169.7 (2017), pp. 1291–1302.
- [2] Nicholas J Audette and David M Schneider. "Stimulus-specific prediction error neurons in mouse auditory cortex". In: *Journal of Neuroscience* 43.43 (2023), pp. 7119–7129.
- [3] Nicholas J Audette et al. "Precise movement-based predictions in the mouse auditory cortex". In: Current Biology 32.22 (2022), pp. 4925–4940.
- [4] Georgia Bastos et al. "Top-down input modulates visual context processing through an interneuron-specific circuit". In: Cell reports 42.9 (2023).
- [5] Rishidev Chaudhuri et al. "A large-scale circuit mechanism for hierarchical dynamical processing in the primate cortex". In: *Neuron* 88.2 (2015), pp. 419–431.
- [6] Cameron Condylis et al. "Dense functional and molecular readout of a circuit hub in sensory cortex". In: Science 375.6576 (2022), eabl5981.

- [7] CPJ De Kock et al. "Layer-and cell-type-specific suprathreshold stimulus representation in rat primary somatosensory cortex". In: *The Journal of physiology* 581.1 (2007), pp. 139–154.
- [8] Shlomo Dellal et al. "Inhibitory and disinhibitory VIP IN-mediated circuits in neocortex". In: bioRxiv (2025).
- [9] Karl Friston. "Does predictive coding have a future?" In: Nature neuroscience 21.8 (2018), pp. 1019–1021.
- [10] Kaitlyn M. Gabhart, Yihan (Sophy) Xiong, and André M. Bastos. "Predictive coding: a more cognitive process than we thought?" In: Trends in Cognitive Sciences (2025). ISSN: 1364-6613. DOI: https://doi.org/10.1016/j.tics.2025.01.012. URL: https://www.sciencedirect.com/science/article/pii/S1364661325000300.
- [11] Aleena R Garner and Georg B Keller. "A cortical circuit for audio-visual predictions". In: *Nature neuroscience* 25.1 (2022), pp. 98–105.
- [12] Marta I Garrido et al. "Dynamic causal modelling of evoked potentials: a reproducibility study". In: Neuroimage 36.3 (2007), pp. 571–580.
- [13] Marta I Garrido et al. "The mismatch negativity: a review of underlying mechanisms". In: Clinical neurophysiology 120.3 (2009), pp. 453–463.
- [14] Jordan P Hamm and Rafael Yuste. "Somatostatin interneurons control a key component of mismatch negativity in mouse visual cortex". In: *Cell reports* 16.3 (2016), pp. 597–604.
- [15] Jordan P Hamm et al. "Cortical ensembles selective for context". In: *Proceedings of the National Academy of Sciences* 118.14 (2021), e2026179118.
- [16] Riitta Hari. "Temporal Aspects of Human Auditory Cortical Processing: Neuromagnetic and Psychoacoustical Data". In: Acoustical Signal Processing in the Central Auditory System. Springer, 1997, pp. 321–328.
- [17] Micha Heilbron and Maria Chait. "Great expectations: is there evidence for predictive coding in auditory cortex?" In: *Neuroscience* 389 (2018), pp. 54–73.
- [18] Loreen Hertäg and Claudia Clopath. "Prediction-error neurons in circuits with multiple neuron types: Formation, refinement, and functional implications". In: *Proceedings of the National Academy of Sciences* 119.13 (2022), e2115699119.
- [19] Adam Hockley, Laura H Bohórquez, and Manuel S Malmierca. "Top-down prediction signals from the medial prefrontal cortex govern auditory cortex prediction errors". In: *Cell Reports* 44.4 (2025).
- [20] Yujie Hou et al. Where, how and why do top-down and bottom-up signals interact in the primate brain? PsyArXiv preprint. 2025. DOI: 10.31234/osf.io/7mryq_v1. URL: https://osf.io/preprints/psyarxiv/7mryq_v1.
- [21] Rebecca Jordan and Georg B Keller. "The locus coeruleus broadcasts prediction errors across the cortex to promote sensorimotor plasticity". In: *Elife* 12 (2023), RP85111.
- [22] Georg B Keller and Thomas D Mrsic-Flogel. "Predictive processing: a canonical cortical computation". In: *Neuron* 100.2 (2018), pp. 424–435.
- [23] Robert T Knight. "Decreased response to novel stimuli after prefrontal lesions in man". In: Electroencephalography and Clinical Neurophysiology/Evoked Potentials Section 59.1 (1984), pp. 9–20.
- [24] Ana B Lao-Rodríguez, David Pérez-González, and Manuel S Malmierca. "Physiological properties of auditory neurons responding to omission deviants in the anesthetized rat". In: *Hearing Research* 452 (2024), p. 109107.
- [25] Ana B Lao-Rodríguez et al. "Neuronal responses to omitted tones in the auditory brain: A neuronal correlate for predictive coding". In: *Science Advances* 9.24 (2023), eabq8657.
- [26] Soohyun Lee et al. "A disinhibitory circuit mediates motor integration in the somatosensory cortex". In: *Nature neuroscience* 16.11 (2013), pp. 1662–1670.
- [27] John Meng and Xiao-Jing Wang. "Global error signal guides local optimization in mismatch calculation". In: bioRxiv (2025), pp. 2025–07.

- [28] Fabian A Mikulasch et al. "Where is the error? Hierarchical predictive coding through dendritic error computation". In: *Trends in Neurosciences* 46.1 (2023), pp. 45–59.
- [29] Beren Millidge, Anil Seth, and Christopher L Buckley. "Predictive coding: a theoretical and experimental review". In: arXiv preprint arXiv:2107.12979 (2021).
- [30] Cristopher M Niell and Michael P Stryker. "Highly selective receptive fields in mouse visual cortex". In: *Journal of Neuroscience* 28.30 (2008), pp. 7520–7536.
- [31] Sean M O'Toole, Hassana K Oyibo, and Georg B Keller. "Molecularly targetable cell types in mouse visual cortex have distinguishable prediction error responses". In: *Neuron* 111.18 (2023), pp. 2918–2928.
- [32] Matthew F Panichello et al. "Intermittent rate coding and cue-specific ensembles support working memory". In: *Nature* (2024), pp. 1–8.
- [33] Carsten K Pfeffer et al. "Inhibition of inhibition in visual cortex: the logic of connections between molecularly distinct interneurons". In: *Nature neuroscience* 16.8 (2013), pp. 1068–1076.
- [34] Rajesh PN Rao and Dana H Ballard. "Predictive coding in the visual cortex: a functional interpretation of some extra-classical receptive-field effects". In: *Nature neuroscience* 2.1 (1999), pp. 79–87.
- [35] Shuzo Sakata and Kenneth D Harris. "Laminar structure of spontaneous and sensory-evoked population activity in auditory cortex". In: *Neuron* 64.3 (2009), pp. 404–418.
- [36] David M Schneider, Anders Nelson, and Richard Mooney. "A synaptic and circuit basis for corollary discharge in the auditory cortex". In: *Nature* 513.7517 (2014), pp. 189–194.
- [37] David M Schneider, Janani Sundararajan, and Richard Mooney. "A cortical filter that learns to suppress the acoustic consequences of movement". In: *Nature* 561.7723 (2018), pp. 391–395.
- [38] Michael N Shadlen and William T Newsome. "Neural basis of a perceptual decision in the parietal cortex (area LIP) of the rhesus monkey". In: *Journal of neurophysiology* 86.4 (2001), pp. 1916–1936.
- [39] Shan Shen et al. "Distinct organization of two cortico-cortical feedback pathways". In: *Nature communications* 13.1 (2022), p. 6389.
- [40] Yuriy Shymkiv et al. "Slow cortical dynamics generate context processing and novelty detection". In: Neuron (2025).
- [41] Adam C Snyder, M Yu Byron, and Matthew A Smith. "A stable population code for attention in prefrontal cortex leads a dynamic attention code in visual cortex". In: *Journal of Neuroscience* 41.44 (2021), pp. 9163–9176.
- [42] Magdalena Solyga and Georg B Keller. "Multimodal mismatch responses in mouse auditory cortex". In: *eLife* 13 (2025), RP95398.
- [43] Michael W Spratling. "A review of predictive coding algorithms". In: *Brain and cognition* 112 (2017), pp. 92–97.
- [44] Kenneth C Squires et al. "The effect of stimulus sequence on the waveform of the cortical event-related potential". In: *Science* 193.4258 (1976), pp. 1142–1146.
- [45] Mark G Stokes. "Activity-silent'working memory in prefrontal cortex: a dynamic coding framework". In: *Trends in cognitive sciences* 19.7 (2015), pp. 394–405.
- [46] Mariko Tada et al. "Mismatch negativity (MMN) as a tool for translational investigations into early psychosis: A review". In: *International Journal of Psychophysiology* 145 (2019), pp. 5–14.
- [47] Robin Tremblay, Soohyun Lee, and Bernardo Rudy. "GABAergic interneurons in the neocortex: from cellular properties to circuits". In: *Neuron* 91.2 (2016), pp. 260–292.
- [48] Catherine Wacongne, Jean-Pierre Changeux, and Stanislas Dehaene. "A neuronal model of predictive coding accounting for the mismatch negativity". In: *Journal of Neuroscience* 32.11 (2012), pp. 3665–3678.
- [49] X-J Wang et al. "Division of labor among distinct subtypes of inhibitory neurons in a cortical microcircuit of working memory". In: *Proceedings of the National Academy of Sciences* 101.5 (2004), pp. 1368–1373.

- [50] Felix C Widmer, Sean M O'Toole, and Georg B Keller. "NMDA receptors in visual cortex are necessary for normal visuomotor integration and skill learning". In: *Elife* 11 (2022), e71476.
- [51] Kong-Fatt Wong and Xiao-Jing Wang. "A recurrent network mechanism of time integration in perceptual decisions". In: *Journal of Neuroscience* 26.4 (2006), pp. 1314–1328.
- [52] Siyu Zhang et al. "Long-range and local circuits for top-down modulation of visual cortex processing". In: *science* 345.6197 (2014), pp. 660–665.
- [53] Pawel Zmarz and Georg B Keller. "Mismatch receptive fields in mouse visual cortex". In: *Neuron* 92.4 (2016), pp. 766–772.

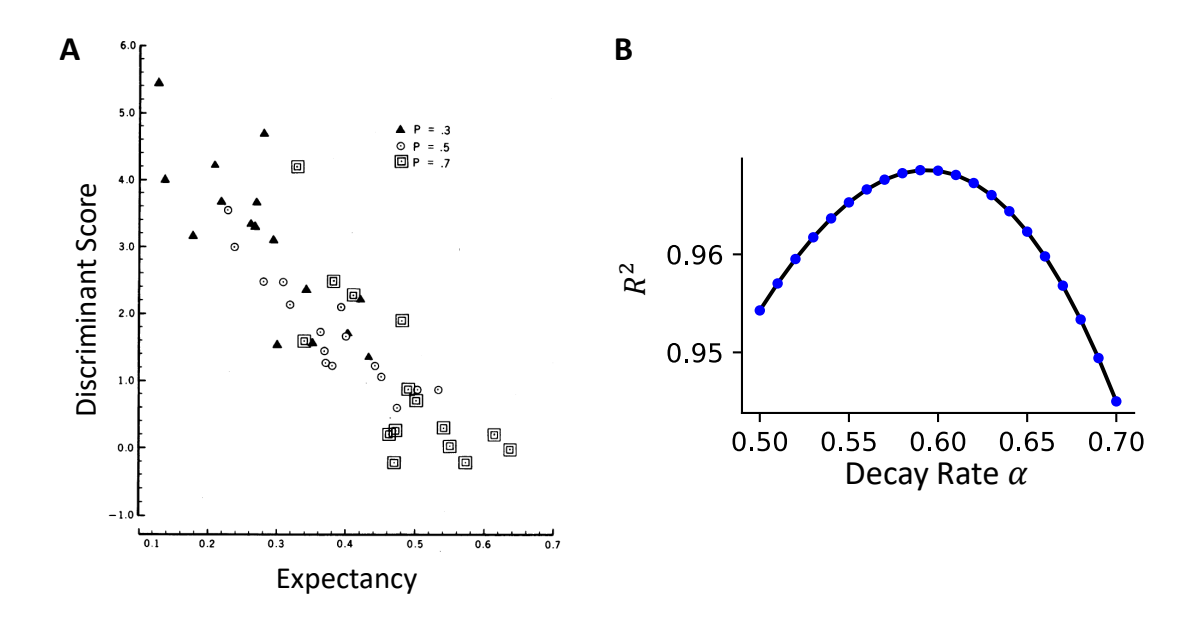


Fig. 7 Related to figure 3. (A) Model behavior is best captured with a memory decay rate of $\alpha=0.6$. The y-axis shows the variance explained by a linear fit between the difference in population-averaged activity and the computed expectancy. (B) Relationship between discriminant score and expectancy, reproduced from [44] with permission. The discriminant score is calculated based on the N200, P300, and slow waveform components. Expectancy is computed using a memory decay rate of $\alpha=0.6$.

Supplementary Materials

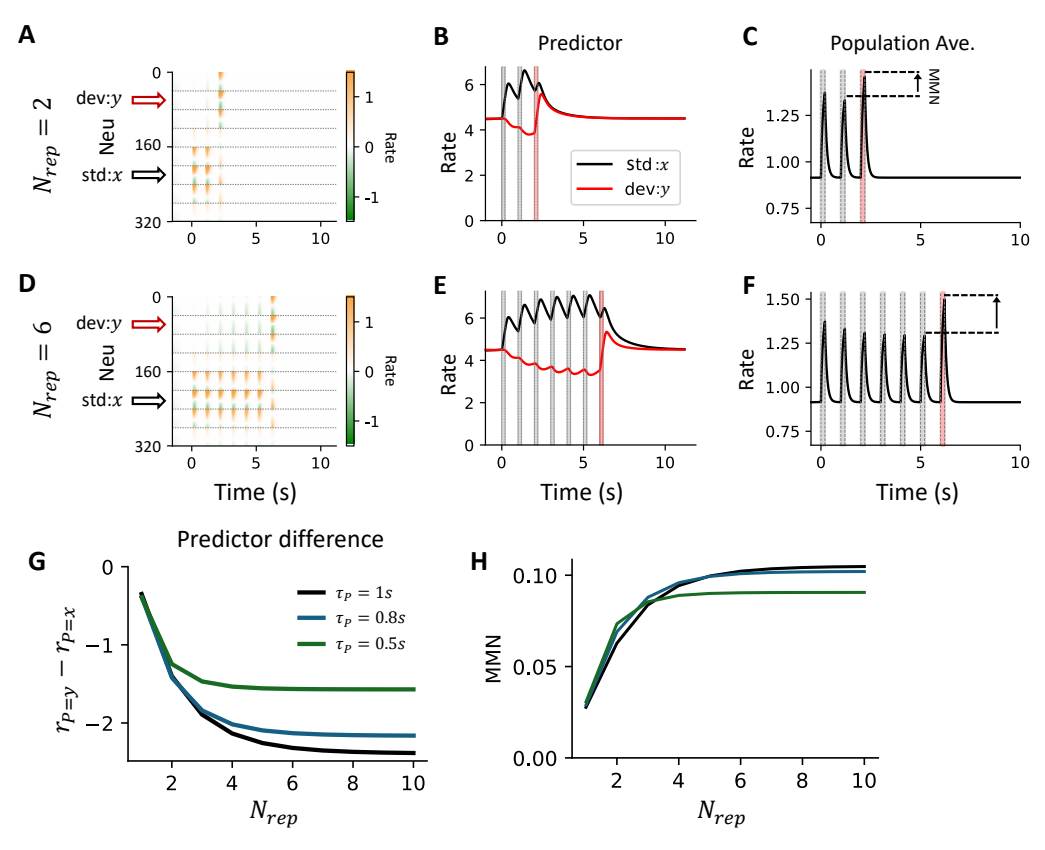


Fig. 8 MMN increases with the number of repetitions N_{rep} . Related to figure 3. (A) Activity of individual neurons with two repetitions of the standard stimulus ($N_{rep} = 2$). (B) Predictor activity for both standard and deviant stimuli. (C) Average population activity over time. (D to F) Same as (A to C) but with six repetitions ($N_{rep} = 6$). (G) The difference in predictor activity between deviant and standard stimuli ($r_{P=y} - r_{P=x}$) becomes more negative as the number of repetitions increases. Each color represents a different τ_P value. A longer time constant leads to slower saturation of the predictor signal. (H) MMN increases over the number of repetitions.

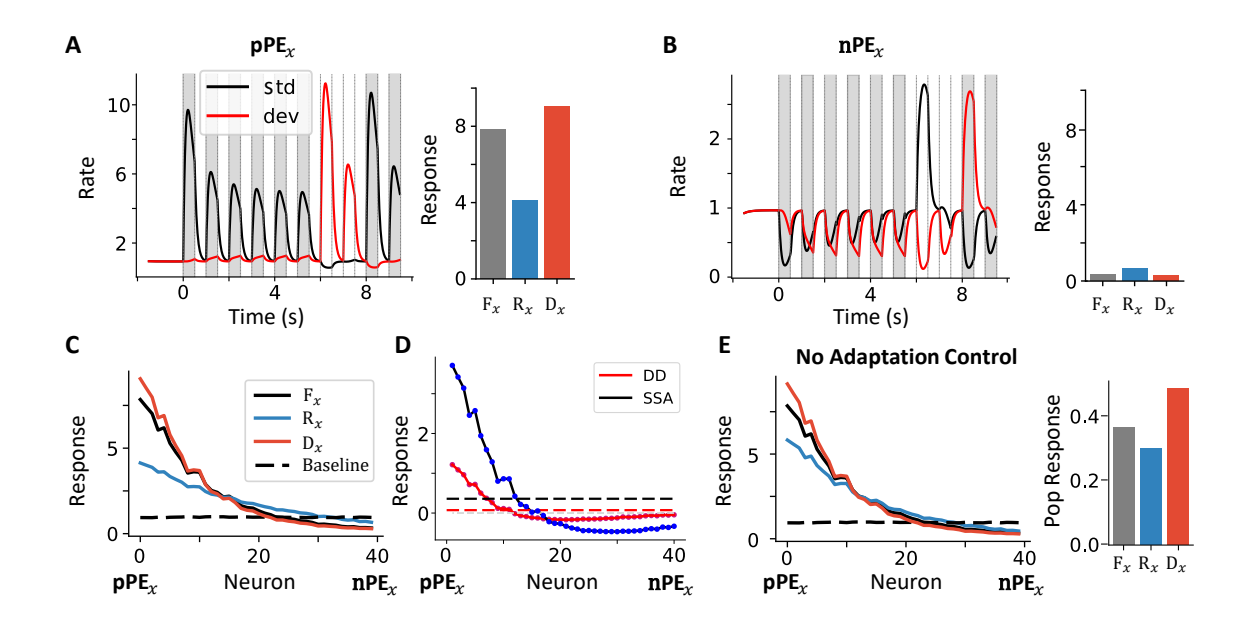


Fig. 9 Individual neuron activity in fixed oddball sequence and no-adaptation control. Related to figure 4. (A) a pPE_x neuron over time when the corresponding stimulus is shown as the standard (black) or deviant stimulus (red). (B) an nPE_x neuron activity. (C) Population response across different contexts. (D) deviance detection (DD, deviant minus first occurrence) and stimulus-specific adaptation (SSA, first minus last repetition) of all the neurons. Dashed lines indicates corresponding average response of the population. (E) No adaptation control. Here, the stimulus is not adapted. See Methods. The individual (left) and averaged population response across all columns (right). Compared to the case with stimulus adaptation, only the activity during the last repetition increases, while the deviant response remains unaffected.

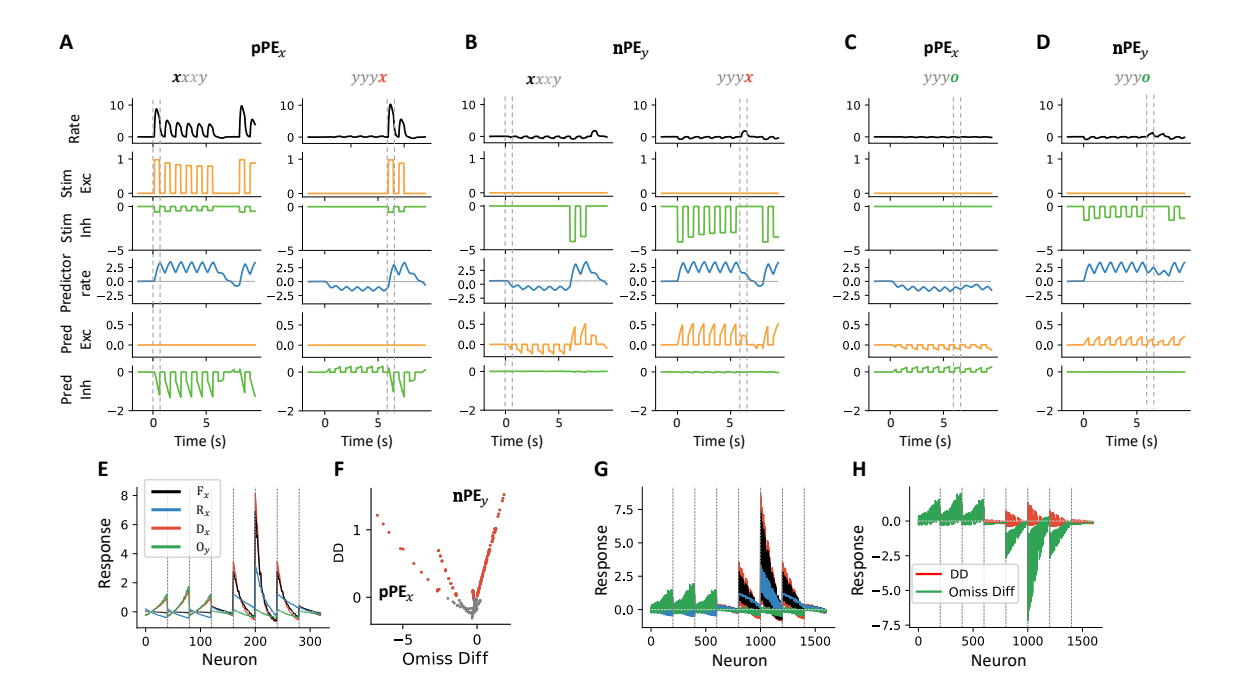


Fig. 10 Input differences across channels between pPE_x and nPE_y neurons. Related to figure 4. (A) Activity of pPE_x during the fixed oddball sequences xxxy and yyyx. From top to bottom: neuron firing rate; somatic excitation, representing stimulus-driven excitation; dendritic inhibition relayed by the I2 population, representing stimulus-driven inhibition; predictor activity selective to stimulus x; dendritic excitation, representing prediction-related excitation; and somatic inhibition relayed by the I1 population, representing prediction-related inhibition. (B) Same as (A), but for a nPE_y . (C, D) Same layout as (A), but in the omission protocol yyyo. (E) Individual neuron responses across contexts. (F) Scatter plot of deviance detection (DD) and omission difference in the simplified model version, which assumes the total maximum input is the same across neurons. (G) Same as (E) but based on results from the realistic model version. (H) Deviance detection and omission difference in the realistic model version (Related to Figure 4J).

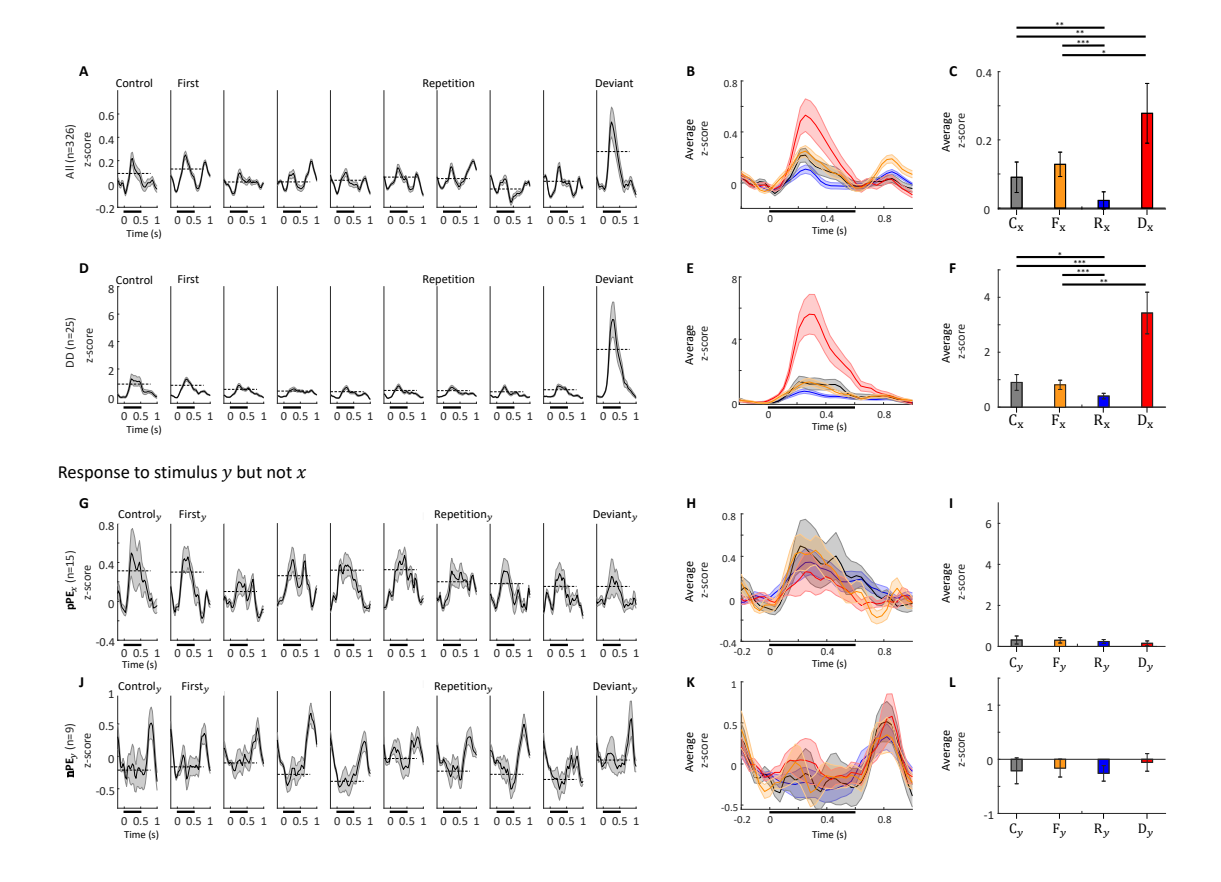


Fig. 11 Further analysis on neurons during randomized oddball protocols. Related to Figure 6. (A) Average z-scored activity of all recorded neurons across different contexts. The black bars below the x-axis indicate the stimulation period. (B) Overlay of neural activity traces across contexts. (C) Mean activity across contexts. (D–F) Same as (A–C), but limited to deviant detectors (n=25). To test whether nPE responses could be attributed to predictors rather than nPE, we examined responses to the perpendicular stimulus y instead of the tested stimulus x across different contexts in the following: (G–I) Same as (A–C), but for pPE $_x$ responses to stimulus y. No significant differences are observed across contexts. (J–L) Same as (G–I), but for nPE $_y$ neurons. Again, no significant differences are found across contexts. *: p < 0.05; **: p < 0.01; ***: p < 0.001. Detailed p-values are reported in the Supplementary Materials.

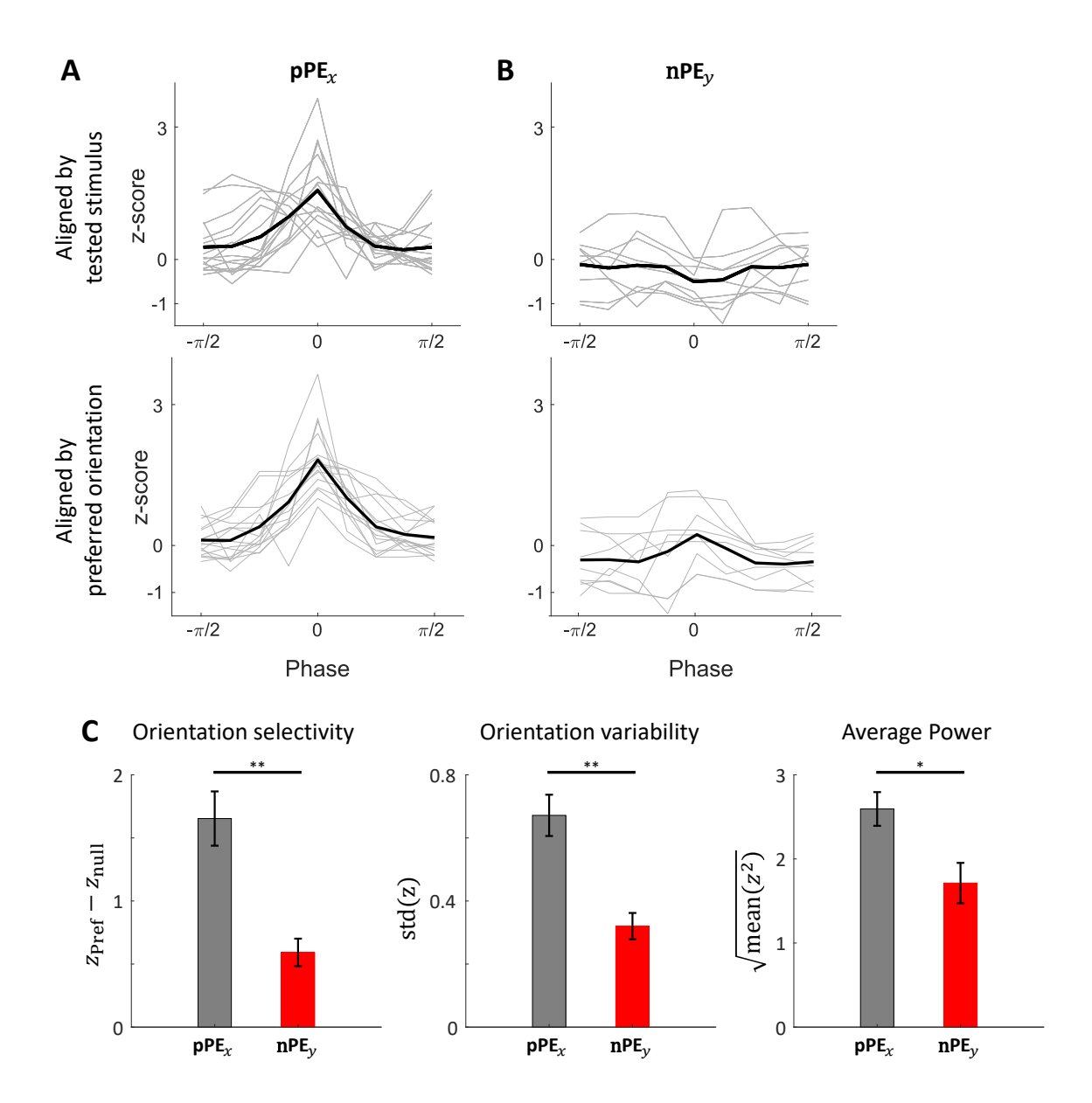


Fig. 12 Tuning curves of pPE_x and nPE_y neurons. Related to Figure 6. (A) Average z-scored responses to different stimulus orientations for pPE_x neurons. Gray lines represent tuning curves for individual neurons; the black line shows the population average. (Top) The tuning curves are aligned with the tested stimulus x in the oddball protocols. (Bottom) The same tuning curves aligned with the preferred orientation of each neuron. (B) Same as (A), but for nPE_y neurons. (C) Orientation selectivity index for pPE_x and nPE_y neurons, calculated as the z-score at the preferred orientation minus the z-score at the orthogonal (null) orientation. Error bars represent the standard deviation of the mean. Note that the preferred orientation is not necessarily 0 degree. **: p < 0.01. (D) Orientation variability, measured as the standard deviation of z-scores across all tested orientations. (E) Average response power, computed as the geometric mean of z-scores across orientations. *: p < 0.05.